Crystal Structure, Magnetic Properties, and Single-Crystal EPR Spectra of a $[CuNi]_2$ Bis Heterobinuclear Compound: Complementarity of the Magnetic and EPR Techniques

Yves Journaux,[†] Olivier Kahn,*[†] Irene Morgenstern-Badarau,[†] Jean Galy,*[‡] Joël Jaud,[‡] Alessandro Bencini,[§] and Dante Gatteschi*[§]

Contribution from the Laboratoire de Spectrochimie des Elêments de Transition, Unité Associee au CNRS n° 420, Universite de Paris-Sud, 91405 Orsay, France, the Laboratoire de Chimie de Coordination, Associee a l'Universite Paul Sabatier, 31030 Toulouse, France, and the Department of Chemistry, University of Florence, and the ISSECC, CNR, Florence, Italy.
Received April 4, 1985

Abstract: The compound Cu(salen)Ni(hfa)$_2$ where salen is *N,N'*-ethylenebis(oxosalicyldiiminato) and hfa is hexafluoroacetylacetonato has been synthesized and its crystal structure has been solved at -123 K. It crystallizes in the monoclinic system, space group $P2_1/c$: a = 9.287 (4) Å, b = 21.533 (2) Å, c = 14.733 (3) Å, β = 94.36 (3)° with Z = 4 CuNi units. The copper is in a planar environment and the nickel in a distorted octahedral environment. The CuO_2Ni bridging angle is bent with a dihedral angle of 141.4°. Two CuNi units of this kind are related through a symmetry center, giving rise to a remarkable [Cu(salen)Ni(hfa)$_2$]$_2$ entity with a relatively short copper-copper separation, 3.432 (1) Å. The magnetic properties of this compound have been studied in the 1.27-300 K temperature range. They correspond to what is expected for an antiferromagnetically coupled CuNi pair with $S_{Cu} = {}^1/_2$ and $S_{Ni} = 1$ local spin. The interaction gives rise to a doublet and a quartet pair state. The doublet state is the lowest and the doublet-quartet splitting is 35.4 cm^{-1}. In contrast, the EPR properties are entirely associated with the bis heterobimetallic entity. The EPR spectrum is that of a triplet state arising from the interaction between two doublet pair states. A single-crystal EPR investigation has been carried out at X-band frequency, at 4.2 K. The principal values and the orientations of the **g** and **D** tensors associated with the triplet state have been determined. A model is presented, allowing the calculation of the dipolar contribution, which is found to be much larger than the experimental **D** tensor. The difference is ascribed to both the specific nature of the interacting doublet states and the anisotropic exchange. Finally, the complementarity of the magnetic and EPR techniques is emphasized. The magnetic properties lead to the interaction between copper(II) and nickel(II) within the CuNi unit, and the EPR properties specify the interaction between two symmetry-related units within the bis heterobinuclear entity.

The field of heteropolymetallic systems is likely that where the complementarity of the magnetic and EPR technique is the most evident.[1-5] By simplifying, we can say that the magnetic properties lead to the spin states of the low-lying levels and to their relative energies and that the EPR studies allow us to specify the details of these low-lying levels, in particular the role of small effects like local and exchange anisotropies.

The accuracy on the determination of the energy gaps between the low-lying levels from the magnetic properties depends on the number of these low-lying levels. It is clear that the most favorable situation is that where only two levels are thermally accessible. In such a case, the theoretical expression of the magnetic susceptibility only depends on the energy gap between these states, which is a physical observable and not a simple phenomenological exchange parameter. Such a situation occurs in the bimetallic complexes where one of the interacting ions is copper(II) and the other one any ion without first-order angular momentum.[4] The copper(II)-nickel(II) heterobimetallic complexes enter into this category, and so far several compounds of this kind have been investigated. For two of them, both magnetic and EPR data have been reported.[2,3,5] In one case, only magnetic properties have been investigated.[6] In other cases, the authors focused on the EPR study of doped species.[7-11] The interaction between the doublet single-ion ground state for copper(II) and the triplet single-ion ground state for nickel(II) gives rise to two molecular states, a doublet and a quartet, separated by an energy $\Delta = -3J/2$ where J is the parameter involved in the exchange Hamiltonian $-J\hat{S}_{Cu}\cdot\hat{S}_{Ni}$. In all the reported cases of pure heterobimetallic systems, the interaction is antiferromagnetic so that the doublet state is the lowest as shown by the magnetic properties and/or the shape and the temperature dependence of the EPR spectra. In principle, both the $S = {}^1/_2$ and $S = {}^3/_2$ states are EPR-active since the former is constituted by a single Kramers doublet and the latter by a pair of Kramers doublets. In fact, so far, only the signals associated with the $S = {}^1/_2$ ground state have been actually detected. Likely, the excited quartet state is too high in energy so that in the temperature range where this state is thermally populated, the relaxation time is too short. Actually, all the EPR studies dealt with CuNi complexes with a planar $Cu(O)_2Ni$ network, which has been shown to lead to a strong antiferromagnetic interaction.[2] The doublet-quartet energy gap was found as -213 cm^{-1} in CuNi(fsa)$_2$en(H$_2$O)$_2$·2H$_2$O[2] and as -309 cm^{-1} in CuNiLCl$_2$·2H$_2$O where L is the binucleating Robson ligand.[5] In the hope of detecting the quartet state in EPR, we decided to investigate a CuNi pair in which the antiferromagnetic interaction would be less pronounced. Such a situation is in principle expected with a bent bridging network as those obtained in the bimetallic complexes resulting from the condensation of a tetradentate Schiff base complex and a hexafluoroacetylacetonato complex.[6,12,13]

[†] Université de Paris-Sud.
[‡] Associée à l'Université Paul Sabatier.
[§] University of Florence.

(1) See, for instance: "Magneto-Structural Correlations in Exchange Coupled Systems"; Willet, R. D., Gatteschi, D., Kahn, O. Eds.; by D. Reidel: Dordrecht, 1984; NATO ASI Ser.
(2) Morgenstern-Badarau, I.; Rerat, M.; Kahn, O.; Jaud, J.; Galy, J. *Inorg. Chem.* **1982**, *21*, 3050-3059.
(3) Desjardins, S.; Morgenstern-Badarau, I.; Kahn, O. *Inorg. Chem.* **1984**, *23*, 3833-3835.
(4) Journaux, Y.; Kahn, O.; Zarembowitch, J.; Galy, J.; Jaud, J. *J. Am. Chem. Soc.* **1983**, *105*, 7585-7591.
(5) Lambert, S. L.; Spiro, C. L.; Gagné, R. R.; Hendrickson, D. N. *Inorg. Chem.* **1982**, *21*, 68-72.
(6) O'Connor, C. J.; Freyberg, D. P.; Sinn, E. *Inorg. Chem.* **1979**, *18*, 1077-1088.
(7) Kokoszka, G. F.; Allen, H. C., Jr.; Gordon, G. *J. Chem. Phys.* **1967**, *46*, 3020-3024.
(8) Bullugiu, E. *J. Phys. Chem. Solids* **1980**, *41*, 1175-1180.
(9) Banci, L.; Bencini, A.; Dei, A.; Gatteschi, D. *Inorg. Chem.* **1981**, *20*, 393-398.
(10) Banci, L.; Bencini, A.; Benelli, C.; Dei, A.; Gatteschi, D. *Inorg. Chem.* **1981**, *20*, 1399-1402.
(11) Bencini, A.; Benelli, C.; Gatteschi, D.; Zanchini, C. *J. Am. Chem. Soc.* **1980**, *102*, 5820-5823.
(12) O'Bryan, N. B.; Maier, T. O.; Paul, I. C.; Drago, R. S. *J. Am. Chem. Soc.* **1973**, *95*, 6640-6645.

0002-7863/85/1507-6305$01.50/0

Accordingly, we synthesized the complex Cu(salen)Ni(hfa)$_2$. The magnetic properties show that, as expected, the doublet–quartet splitting is weaker than in the CuNi pairs with a planar bridging network. As for the EPR spectra, they are quite surprising at first view. They correspond neither to a ground doublet state, nor to an excited quartet state, nor to a superposition of the two kinds of spectra. Actually the spectra correspond to a very low-lying triplet state arising from the interaction between the two $S = {}^1/_2$ ground states of the Cu(salen) Ni(hfa)$_2$ moities related in the crystal by an inversion center. The goal of this paper is to exploit fully the complementarity of the informations coming from magnetic susceptibility and EPR spectra to understand the nature of the ground manifold of energy levels, taking explicitly into account exchange and dipolar interactions as well as the role of the local anistropy of the nickel(II) ion in determining the relative energies of these levels.

Experimental Section

Synthesis. The *N,N'*-ethylenebis(oxosalicyldiiminato) Cu(salen) was prepared as described in ref 1 by replacing the cobalt(II) acetate by the copper(II) acetate. The bis(hexafluoacetylacetonato)nickel Ni(hfa)$_2$-(H$_2$O)$_2$ was obtained as described in ref 15 by using nickel(II) acetate instead of copper(II) acetate.

To a solution of 660 mg (2×10^{-3} mol) of Cu(salen) dissolved in 50 mL of chloroform is added 1.018 g (2×10^{-3} mol) of Ni(hfa)$_2$(H$_2$O)$_2$ dissolved in the minimum of methanol. The resulting solution is then heated at reflux during 10 min and progressively becomes red. Large and well-shaped single crystals of Cu(salen)Ni(hfa)$_2$ were obtained by slow evaporation of the filtered solution. Anal. Calcd for $C_{26}H_{16}O_6N_2F_{12}CuNi$: C, 38.91; H, 2.01; N, 3.49; F, 28.4. Found: C, 38.90; H, 1.98; N, 3.44; F, 27.7.

X-ray Analysis. Structure Determination. A single crystal having the shape of a regular block was selected. The crystal system, monoclinic, the space group, $P2_1/c$, as well as approximate unit cell parameters were determined from the Buerger diagrams using a zirconium filtered molybdenum radiation. The crystal was then mounted on a CAD 4 Enraf Nonius PDP 8/M computer-controlled diffractometer and the unit cell parameters were refined by optimizing the settings of 25 reflections at two temperatures, namely 293 and 123 K. The results are shown in Table I, as well as the schedule for the measurement of the intensity of the reflections. Lorentz and polarization factors were applied, but owing to the shape of the crystal, absorption corrections were estimated not to be necessary. Atomic scattering factors of Cromer and Waber[16] for the non-hydrogen atoms and those of Stewart, Davidson and Simpson[17] for the spherical hydrogen atoms were used. Real and imaginary dispersion corrections given by Cromer were applied for all the non-hydrogen atoms. When a set of data collected at room temperature was used, the structure was determined by deconvolution of the Patterson function followed by a Fourier synthesis. This gave the general shape of the molecular structure; anyhow, it was impossible to localize both the fluorine and hydrogen atoms, in spite of a rather low reliability factor, i.e., $R = 0.12$. It was then decided to collect a new set of data at 123 K in order to freeze the thermal vibrations. On a subsequent Fourier difference using these new data, three CF_3 groups (C(4)F$_3$, C(5)F$_3$, and C(9)F$_3$) were easily detected, the remaining one C(10)F$_3$ being still disordered with fluorine atoms delocalized over three crystallographically independent positions. All the hydrogen atom positions were also determined. Concerning the C(10)F$_3$ group, it is to be noticed that the occupancy factors of the three positions are not equivalent, these factors being 0.60, 0.25, and 0.15. The refinement conducted in such conditions quickly dropped to $R = 0.042$ and $R_w = 0.043$. All non-hydrogen atoms were allowed to refine with anisotropic thermal parameters, the disordered fluorine atoms with intercorrelated isotropic thermal parameters, and the hydrogen atoms with a fixed isotropic thermal parameter of $B_H = 1.2$ B equiv (C) Å^2; B equiv (C) $= {}^4/_3\sum\sum_{ij}[(a_i a_j)\beta_{ij}]$ is the isotropic equivalent factor of the carbon to which the hydrogen atom is bound. The last difference Fourier map showed no peak greater than 0.2 Å^{-3}.

Positional parameters are given in Tables II, VI and VII. Bond lengths and bond angles are given in Table III.

Table I. Information Concerning Crystallographic Data Collection

cryst syst	monoclinic	monoclinic
	Crystallographic and Physical Data	
temp, K	123	293
a, Å	9.287 (4)	9.455 (5)
b, Å	21.533 (2)	21.709 (4)
c, Å	14.733 (3)	14.976 (4)
β, deg	94.36 (3)	95.23 (6)
M_r	802.66	
V, Å^3	2937.8 (7)	3061 (1)
Z	4	4
$F(000)$	1596	1596
ρ_{exptl}, g cm^{-3}		1.70 (5)
ρ_x, g cm^{-3}	1.82	1.74
abs. factor, cm^{-1}	13.3	
morphology	littl reg block, max and min size (mm) 0.32, 0.28	
	Data Collection	
temp, K	123	
radiat	Mo Kα	
monochromatizat	grapite monochromat	
λ(Kα)	0.710 69	
cryst detector distn, mm	207	
detector window ht and width, mm	4.4	
take-off angle, deg	2.75	
scan ang for ω ang, deg	$0.8 + 0.347tg\theta$	
scan mode	$\theta - \theta$	
max Bragg ang, deg	30	
val determ scan speed		
SIGPRE	0.750	
SIGMA	0.018	
VPRE, deg min^{-1}	6.7	
TMAX, s	85	
control refl		
intens, periodic 3600 s	$1\bar{3}5$, $25\bar{7}$, $47\bar{1}$	
orientat after 100 refl.	$1,\bar{1}5,\bar{1}$; 0,15,3; 008	
	Conditions for Refinement	
refl for the refinement of the cell dimens	25	
recorded refl	9118	
utilized refl	6133 ($I > 3\sigma(I)$)	
refined param	435	
reliability factors		
$R = \sum\|k\|F_o\| - \|F_c\|\|/\sum k\|F_o\|$	0.042	
$R_w = [\sum w(k\|F_o\| - \|F_c\|)^2/\sum wk^2F_o^2]^{1/2}$	0.043	
$w = 4F_o^2/\sigma^2(F_o)^2$		

Magnetic Measurements. The magnetic susceptibility of Cu(salen)-Ni(hfa)$_2$ was measured in two stages, with a Faraday-type magnetometer equipped with a He continuous flow cryostat in the 4.2–300 K temperature range and with a mutual inductance bridge magnetometer in the 1.27–4.2 temperature range. Above 4.2 K, we used samples weighing about 10 mg and magnetic fields of about 3000 G. Below 4.2 K, we used a sample of 438 mg and a magnetic field of a few gauss. The diamagnetic correction was estimated as -407×10^{-6} cm^3 mol^{-1}.

EPR. The morphology of the crystal used in the EPR study is shown in Figure 3, as well as the orientation of the crystal axes determined with a Weissenberg camera. This study was carried out at *X*-band frequency with a Bruker ER 200 D spectrometer equipped with a He continuous flow cryostat, a Hall probe, and a frequency meter. The spectra were recorded at 4.2 K in the three orthogonal planes *ab*, *bc**, and *ac**, the crystal being fixed on a vertical Perspex rod able to rotate around its axis. In the *ab* and *bc** planes, the orientation of the crystal was refined by taking advantage of the symmetry around the *b* axis required by the monoclinic space group. In the *ac** plane, the orientation of the crystal was refined by adjusting the values of the resonant fields along the *a* and *c** axes to the values observed in the *ab* and *bc** planes, respectively.

The principal values and the orientations of the **g** and **D** tensors were determined by minimizing the function $\sum_i(\Delta E_i - h\nu)^2$ where $h\nu$ is the incident quantum and ΔE_i the energy differences between the levels involved in the transitions. The energies E_i were calculated for each experimental field by diagonalizing the matrix associated with the Hamiltonian (eq 3) given under the EPR spectra.

Description of the Structure

A perspective view of Cu(salen)Ni(hfa)$_2$ is shown in Figure 1 with the labeling of the atoms. The two fragments, Cu(salen) and Ni(hfa)$_2$, are held together through the phenolic oxygen atoms

(13) Lelie, K. A.; Drago, R. S.; Stucky, G. D.; Kitko, D. J.; Breese, J. A. *Inorg. Chem.* **1979**, *18*, 1885–1891.
(14) Bailes, R. H.; Calvin, M. *J. Am. Chem. Soc.* **1947**, *69*, 1886–1893.
(15) Bedford, R. L.; Martell, A. E.; Calvin, M. J. *Inorg. Nucl. Chem.* **1956**, *2*, 11–31.
(16) Cromer, D. T.; Waber, J. T. *Acta Crystallogr.* **1965**, *18*, 104–109.
(17) Stewart, R. F.; Davidson, E. R.; Simpson, W. T. *J. Chem. Phys.* **1965**, *42*, 3175–3187.

Table II. Final Least-Squares Atomic Coordinates with Estimated Standard Deviations for CuNiF12O6N2O26H16

atom	*x/a*	*y/b*	*z/c*
Cu(1)	0.410 78 (4)	−0.009 74 (2)	0.596 82 (3)
Ni(1)	0.340 96 (4)	0.106 68 (2)	0.681 75 (3)
O(1)	0.293 2 (2)	0.059 20 (9)	0.561 6 (1)
O(2)	0.523 0 (2)	0.050 41 (9)	0.666 0 (1)
O(3)	0.280 2 (2)	0.031 03 (9)	0.753 3 (1)
O(4)	0.397 8 (2)	0.151 1 (1)	0.799 1 (1)
O(5)	0.147 3 (2)	0.148 1 (1)	0.685 0 (1)
O(6)	0.421 2 (3)	0.180 84 (9)	0.619 7 (1)
N(5)	0.297 4 (3)	−0.067 5 (1)	0.523 2 (2)
N(6)	0.525 0 (3)	−0.079 3 (1)	0.637 3 (2)
F(14)	0.319 5 (2)	−0.083 81 (9)	0.813 7 (1)
F(24)	0.143 3 (2)	−0.049 0 (1)	0.884 8 (2)
F(34)	0.356 2 (3)	−0.052 7 (1)	0.951 9 (1)
F(15)	0.347 0 (3)	0.227 1 (1)	0.941 1 (2)
F(25)	0.412 5 (4)	0.155 4 (1)	1.035 3 (2)
F(35)	0.563 6 (3)	0.195 4 (1)	0.950 9 (2)
F(19)	−0.028 0 (3)	0.289 7 (1)	0.706 3 (2)
F(29)	−0.119 3 (3)	0.205 3 (1)	0.651 4 (2)
F(39)	−0.035 7 (3)	0.209 8 (1)	0.791 2 (2)
F(110)	0.507 8 (5)	0.320 7 (2)	0.661 8 (2)
F(210)	0.381 9 (4)	0.325 8 (2)	0.538 2 (3)
F(310)	0.543 8 (5)	0.267 6 (2)	0.526 3 (3)
F(410)	0.596 8 (6)	0.278 9 (9)	0.624 1 (8)
F(510)	0.588 9 (6)	0.266 5 (5)	0.568 0 (8)
F(610)	0.398 (1)	0.341 2 (3)	0.574 8 (8)
F(710)	0.468 (2)	0.278 3 (8)	0.501 5 (3)
F(810)	0.570 (2)	0.298 3 (9)	0.652 6 (9)
F(910)	0.446 (2)	0.342 0 (4)	0.628 (1)
C(1)	0.308 6 (3)	0.025 0 (1)	0.837 2 (2)
C(2)	0.354 2 (4)	0.069 4 (1)	0.901 9 (2)
C(3)	0.389 9 (3)	0.129 5 (1)	0.876 9 (2)
C(4)	0.282 4 (4)	−0.040 8 (1)	0.872 8 (2)
C(5)	0.427 9 (5)	0.176 7 (2)	0.952 5 (2)
C(6)	0.133 2 (4)	0.205 8 (1)	0.679 8 (2)
C(7)	0.230 8 (4)	0.249 9 (1)	0.652 1 (2)
C(8)	0.365 0 (4)	0.233 3 (1)	0.623 7 (2)
C(9)	−0.014 4 (4)	0.228 0 (2)	0.706 9 (2)
O(10)	0.460 7 (3)	0.286 3 (1)	0.590 6 (2)
O(11)	0.194 1 (3)	0.062 2 (1)	0.491 7 (2)
C(12)	0.137 5 (3)	0.120 1 (1)	0.464 7 (2)
C(13)	0.038 4 (4)	0.125 2 (2)	0.390 3 (2)
C(14)	−0.010 6 (4)	0.072 9 (2)	0.341 7 (2)
O(15)	0.043 1 (4)	0.015 8 (2)	0.367 9 (2)
O(16)	0.146 1 (3)	0.008 7 (2)	0.441 5 (2)
O(21)	0.624 5 (3)	0.036 9 (1)	0.732 1 (2)
C(22)	0.694 5 (4)	0.086 0 (2)	0.779 7 (2)
O(23)	0.796 7 (4)	0.075 4 (2)	0.850 8 (3)
C(24)	0.834 9(4)	0.015 1 (2)	0.876 3 (3)
C(25)	0.772 0 (4)	−0.033 7 (2)	0.828 8 (2)
C(26)	0.667 8 (4)	−0.024 7 (1)	0.755 6 (2)
C(51)	0.197 0 (4)	−0.053 6 (1)	0.463 0 (2)
C(52)	0.335 3 (4)	−0.132 5 (2)	0.546 4 (3)
C(61)	0.619 2 (4)	−0.079 0 (1)	0.705 0 (2)
O(62)	0.492 8 (4)	−0.135 0 (1)	0.581 7 (3)

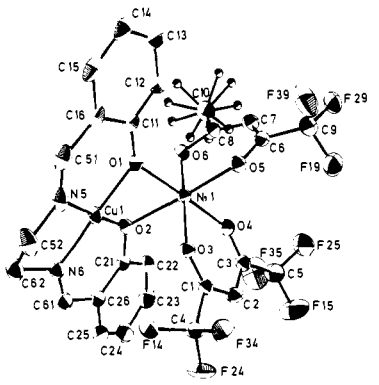

Figure 1. Perspective view of the Cu(salen)Ni(hfa)$_2$ unit.

O1 and O2. In the Cu(salen) fragment, the copper atom is in a square-planar environment with very similar copper–nitrogen

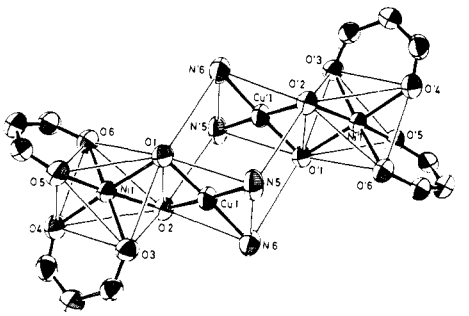

Figure 2. Schematic representation of the bis heterobinuclear entity [Cu(salen)Ni(hfa)$_2$]$_2$.

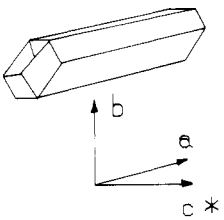

Figure 3. Morphology of the crystal used in the EPR study and orientation of the crystal axes.

and copper–oxygen bond lengths, from 1.892 (2) to 1.914 (2) Å. As for the nickel atom, it is coordinated to six oxygen atoms situated at the corners of a slightly distorted octahedron with the nickel–oxygen bond lengths ranging in the narrow range 2.011 (2) to 2.107 (2) Å. The distance O1–O2 between the bridging atoms is 2.542 (3) Å: it is shorter than all the other O–O distances, which indicates that some repulsion between the metallic ions has occurred. The octahedron Ni1010203040506 is significantly tipped toward the square Cu10102N5N6. Indeed, the oxygen atom O3 comes above the copper atom at a distance of 2.825 (4) Å and the dihedral angle between the equatorial plane Ni101020405, and the basal plane Cu10102N5N6 is only 141.4°, the Cu1–Ni1 separation being shortened to 2.897 (1) Å. The Cu101Ni1 and Cu102Ni1 bridging angles are equal to 94.08 (1)° and 93.70°, respectively. All the structural features described above are rather similar to what has been found in Cu(salen)-Co(hfa)$_2$.[11] However, in this latter compound, the bridging network is less bent than in the title compound; the dihedral angle between the planes containing the metal ions and sharing an edge is 161.9° instead of 141.4°. Accordingly, the Cu–Co separation is significantly longer than the Cu–Ni one, 3.060 (1) Å instead of 2.897 (1) Å. The third M(salen)M′(hfa)$_2$ compound of which the structure is known is that with M = M′ = Cu.[13] This compound has two crystallographically independent molecular units with, in each unit, a very large tetragonal elongation of the six-coordinate environment of the copper atom surrounded by the hfa ligands, leading to a strongly distorted CuO_2Cu bridging network. The structure of Cu(salen)Ni(hfa)$_2$ has also to be compared to that of $CuNi(fsa)_2en(H_2O)_2H_2O$ where the copper and nickel atoms are in similar planar and octahedral surroundings, respectively.[2] In this latter compound, however, the CuO_2Ni network is rigorously planar with CuONi bridging angles of 98.9° and a Cu–Ni separation of 2.9749 (6) Å.

The most important feature of the structure is related to the repetition of the Cu(salen)Ni(hfa)$_2$ unit by a symmetry center located at 1.716 Å of the copper atom, almost on the axis perpendicular to the 0102N5N6 plane and containing the metal center. This gives rise to a remarkable bis heterobinuclear entity, as shown in Figure 2, making a kind of bicapped square prism 030102N6N5 0′10′2N′6N′50′3. Within this bis heterobinuclear entity, the Cu1–Cu′1 distance is 3.432 (1) Å and the 03Cu1Cu′1 angle is 154.8 (1)°. In Cu(salen)Cu(hfa)$_2$ also, two symmetry-related binuclear entities are relatively close to each other with a distance of 3.575 Å between two copper atoms in the salen environment.[13] In contrast, such a packing does not occur in Cu(salen)Co(hfa)$_2$.[12]

Table III. Selected Interatomic Distances (Å) and Bond Angles (deg)

	Distances		
Cu(1)-O(1)	1.892 (2)	Ni(1)-O(1)	2.064 (2)
Cu(1)-O(2)	1.908 (2)	Ni(1)-O(2)	2.107 (2)
Cu(1)-O(3)	2.825 (2)	Ni(1)-O(3)	2.043 (2)
Cu(1)-N(5)	1.914 (3)	Ni(1)-O(4)	2.011 (2)
Cu(1)-N(6)	1.904 (3)	Ni(1)-O(5)	2.011 (2)
Cu(1)-Cu'(1)	3.432 (2)	Ni(1)-O(6)	2.011 (2)
Cu(1)-Ni(1)	2.897 (2)	O(1)-O(2)	2.542 (3)
O(1)-C(11)	1.329 (3)	O(1)-O(3)	2.900 (3)
C(11)-C(12)	1.400 (4)	O(1)-O(5)	3.030 (3)
C(12)-C(13)	1.382 (2)	O(1)-O(6)	2.976 (3)
C(13)-C(14)	1.392 (5)	O(2)-O(3)	2.711 (3)
C(14)-C(15)	1.372 (6)	O(2)-O(4)	3.200 (3)
C(15)-C(16)	1.399 (4)	O(2)-O(6)	3.025 (3)
C(16)-C(11)	1.421 (4)	O(3)-O(4)	2.867 (3)
O(2)-C(21)	1.334 (4)	O(3)-O(5)	2.949 (3)
C(21)-C(22)	1.402 (5)	O(4)-O(5)	2.765 (3)
C(22)-C(23)	1.378 (5)	O(4)-O(6)	2.744 (3)
C(23)-C(24)	1.390 (6)	O(5)-O(6)	2.875 (3)
C(24)-C(25)	1.369 (5)	O(5)-C(6)	1.252 (4)
C(25)-C(26)	1.406 (5)	C(6)-C(7)	1.395 (5)
C(26)-C(21)	1.421 (4)	C(7)-C(8)	1.391 (5)
C(16)-C(51)	1.451 (5)	O(6)-C(8)	1.248 (4)
N(5)-C(51)	1.272 (4)	O(3)-C(1)	1.251 (3)
C(26)-C(61)	1.442 (4)	C(1)-C(2)	1.392 (4)
N(6)-C(61)	1.275 (4)	C(2)-C(3)	1.393 (5)
N(5)-C(52)	1.477 (4)	O(4)-C(3)	1.244 (4)
N(6)-C(62)	1.472 (4)	C(1)-C(4)	1.538 (4)
C(52)-C(62)	1.515 (5)	C(3)-C(5)	1.530 (5)
N(5)-N(6)	2.612 (4)	C(6)-C(9)	1.533 (5)
O(1)-N(5)	2.788 (3)	C(8)-C(10)	1.548 (4)
O(2)-N(6)	2.825 (3)	C(4)-F(14)	1.335 (4)
O(1)-N'(6)	3.518 (4)	C(4)-F(24)	1.328 (4)
O(2)-N'(5)	3.376 (4)	C(4)-F(34)	1.331 (4)
C(9)-F(19)	1.334 (4)	C(5)-F(15)	1.323 (5)
C(9)-F(29)	1.317 (5)	C(5)-F(25)	1.321 (4)
C(9)-F(39)	1.331 (5)	C(5)-F(35)	1.324 (6)
C(10)(0.60)-F(110)	1.330 (5)		
C(10)(0.60)-F(210)	1.331 (5)		
C(10)(0:60-F(310)	1.329 (5)		
C(10)(0.25)-F(410)	1.331 (7)		
C(10)(0.25)-F(510)	1.331 (8)		
C(10)(0.25)-F(610)	1.329 (7)		
C(10)(0.15)-F(710)	1.331 (6)		
C(10)(0.15)-F(810)	1.339 (9)		
C(10)(0.15)-F(910)	1.330 (9)		
	Angles		
O(1)-Cu(1)-O(2)	83.9 (1)	O(5)-Ni(1)-O(4)	86.9 (1)
O(2)-Cu(1)-N(6)	95.6 (1)	O(5)-Ni(1)-O(6)	91.2 (1)
N(6)-Cu(1)-N(5)	86.3 (1)	O(5)-Ni(1)-O(3)	93.3 (1)
N(5)-Cu(1)-O(1)	94.2 (1)	O(5)-Ni(1)-O(1)	96.1 (1)
O(1)-Cu(1)-N(6)	177.4 (1)	O(5)-Ni(1)-O(2)	169.7 (1)
O(2)-Cu(1)-N(5)	177.5 (1)	O(4)-Ni(1)-O(6)	86.0 (1)
Cu(1)-O(1)-Ni(1)	94.08 (8)	O(4)-Ni(1)-O(3)	90.0 (1)
Ni(1)-O(2)-Cu(1)	93.70 (8)	O(4)-Ni(1)-O(1)	177.0 (1)
		O(4)-Ni(1)-O(2)	102.0 (1)
		O(6)-Ni(1)-O(3)	173.8 (1)
		O(6)-Ni(1)-O(1)	93.8 (1)
		O(6)-Ni(1)-O(2)	94.5 (1)
		O(3)-Ni(1)-O(1)	89.9 (1)
		O(3)-Ni(1)-O(2)	81.6 (1)
		O(1)-Ni(1)-O(2)	75.1 (1)

Magnetic Properties and EPR Spectra

The magnetic behavior of Cu(salen)Ni(hfa)$_2$ is represented in Figure 4, in the form of the temperature dependence of the product $\chi_M \cdot T$ of the molar magnetic susceptibility by the temperature. At room temperature, $\chi_M \cdot T$ is equal to 1.64 cm^3 mol^{-1} K. Upon cooling down, $\chi_M \cdot T$ is first almost constant, then decreases, and finally reaches a plateau below about 10 K with $\chi_M \cdot T = 0.492$ cm^3/mol^{-1} K. This plateau continues down to 1.27 K. This behavior closely follows what is expected for a CuNi pair with local spins $S_{Cu} = {}^1/_2$ and $S_{Ni} = 1$. The interaction within the pair gives rise to a spin doublet and a spin quartet. Below 10 K, the quartet excited state is totally depopulated, so that the magnetic

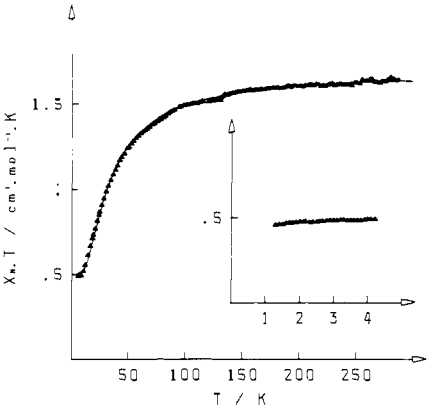

Figure 4. Temperature dependence of $\chi_M \cdot T$ for Cu(salen)Ni(hfa)$_2$: (Δ) experimental data; (—) calculated curve.

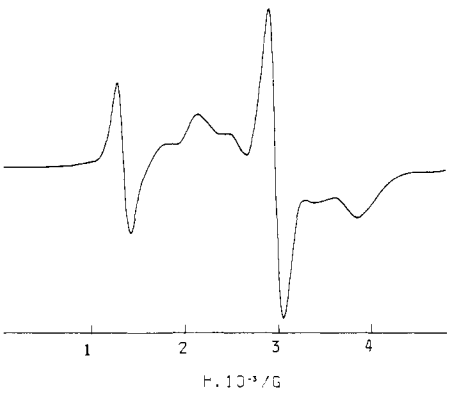

Figure 5. X-band powder spectrum of [Cu(salen)Ni(hfa)$_2$]$_2$ at 4.2 K.

susceptibility follows the Curie law expected for a doublet state. It is quite characteristic that the susceptibility does not deviate significantly from this Curie law, even around the lowest reached temperature, i.e., 1.27 K. This unambigously proves that the interaction between two symmetry-related CuNi pairs is very small. It results that the magnetic data may be interpreted with the theoretical law appropriate for an isolated CuNi pair.[2] This law is

$$\chi_M = \frac{N\beta^2}{4kT} \cdot \frac{\bar{g}_{1/2}{}^2 + 10\bar{g}_{3/2}{}^2 \exp(3J/2kT)}{1 + 2\exp(3J/2kT)} \qquad (1)$$

where $\bar{g}_{1/2}$ and $\bar{g}_{3/2}$ are the average g factors associated with the doublet and quartet states, respectively. In expression 1, we assumed that the eventual zero-field splitting within the quartet state and the coupling of the components of the doublet and quartet states, respectively, were very small with regard to the doublet-quartet splitting $3J/2$. J, $\bar{g}_{1/2}$, and $\bar{g}_{3/2}$ were determined by minimizing the reliability factor $R = \sum[(\chi_M \cdot T)^{obsd} - (\chi_M \cdot T)^{calcd}]^2 / \sum[(\chi_M \cdot T)^{obsd}]^2$ and found as

$$J = -23.6 \text{ cm}^{-1} \quad \bar{g}_{1/2} = 2.30 \quad \bar{g}_{3/2} = 2.22$$

R is then equal to 4.5×10^{-5}.

The powder EPR spectrum of [Cu(salen)Ni(hfa)$_2$]$_2$ at 4.2 K is given in Figure 5. This spectrum vanishes above 20 K. It is evident at first view that it does not correspond to the doublet ground state detected in magnetism for the CuNi pair. Moreover, it cannot be associated with the quartet excited state since this state is totally depopulated at 4.2 K. Actually, it exhibits all the features characteristic of a triplet state without hyperfine structure. Indeed, it shows the allowed transitions $\Delta M_s = \pm 1$ resulting from the zero-field splitting of the triplet state, as well as the forbidden transition $\Delta M_s = 2$ at 1330 G. The absence of hyperfine structure is due to the fact that the magnetic clusters in which the resonances occur are not diluted in a diamagnetic matrix. The Hamiltonian associated with the triplet state may be written

$$\mathcal{H} = \beta \hat{S} \cdot \mathbf{g} \cdot \vec{H} + \hat{S} \cdot \mathbf{D} \cdot S \qquad (2)$$

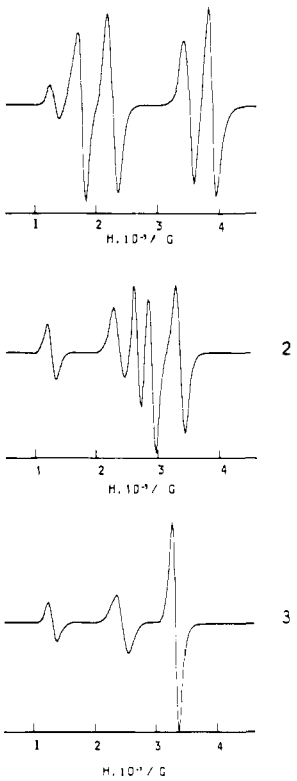

Figure 6. Typical X-band single-crystal EPR spectra of [Cu(salen)Ni(hfa)$_2$]$_2$ at 4.2 K. The spectra refer to the angular settings indicated in Figure 7.

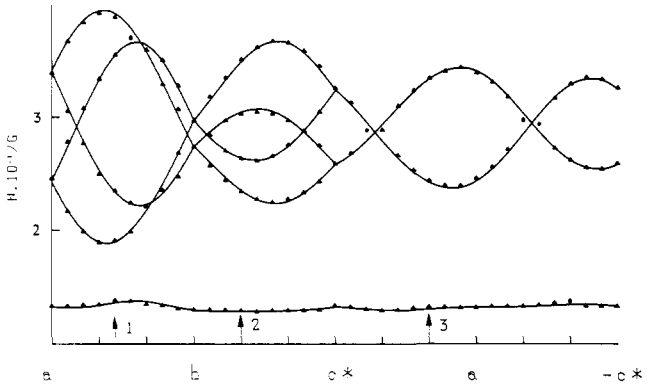

Figure 7. Angular variations of the resonant fields for [Cu(salen)Ni(hfa)$_2$]$_2$: (Δ) experimental data; (—) calculated variations.

For a rhombic system with an axial zero-field-splitting parameter D ($=3D_z/2$) smaller than the incident quantum, six allowed transitions are expected. The spectrum exhibits five peaks including a broad central peak which could result from the superposition of the transitions H_{x_1} and H_{x_2}. If the **g** and **D** tensors in (2) were coincident, their principal values could be calculated from the resonant fields by using Wasserman's equations.[18] In the present case, this has not been possible, which shows that **g** and **D** have not the same principal directions.

The single-crystal study confirms that the observed spectra are those of a triplet state. Three typical spectra are given in Figure 6, and the angular variation of the resonant fields in three orthogonal planes is represented in Figure 7. Owing to the symmetry of the crystal, there are two magnetically nonequivalent sites in the *ab* and *bc** planes but only one site in the *ac** plane and along the *a*, *b*, and *c** directions.[19] In the three planes, the two $\Delta M_s = \pm 1$ transitions per magnetic site are observed. On the other hand, only one $\Delta M_s = 2$ transition is observed in the *ab* and *bc** planes, owing to the weak angular variation of this transition.

Table IV. Principal Values and Orientations with Regard to the *abc** Referential of the **g** and **D** Tensors (Uncertainty on the Last Figure Given in Parentheses; Principal Values of **D** Given in cm^{-1})

	First Fitting			
g_x	2.252 (9)	0.5 (1)	0.71 (4)	0.4 (1)
g_y	2.347 (9)	0.54 (4)	−0.69 (4)	0.47 (4)
g_z	2.227 (9)	0.6 (1)	0.0 (1)	−0.8 (1)
D_x	0.0227 (9)	0.506 (9)	0.28 (1)	−0.81
D_y	0.0606 (9)	−0.323 (9)	−0.769 (4)	−0.50 (1)
D_z	−0.083 (1)	0.768 (3)	−0.576 (3)	0.281 (6)
	Second Fitting			
g_x	2.29 (1)	0.75 (9)	0.05 (9)	0.7 (1)
g_y	2.307 (8)	−0.2 (2)	−0.95 (3)	0.3 (2)
g_z	2.22 (1)	−0.65 (7)	0.31 (8)	0.70 (6)
D_x	−0.02 (1)	−0.382 (9)	0.434 (8)	−0.815 (5)
D_y	−0.076 (1)	0.806 (5)	0.588 (5)	−0.06 (1)
D_z	0.078 (1)	0.452 (5)	−0.682 (4)	−0.575 (6)

To determine the **g** and **D** tensors, there is a difficulty arising from the presence of two magnetic sites in the unit cell. So, to follow the transitions at the junction of the *ab* and *bc** planes, we have the choice between two possibilities. We performed two independent fittings, of which the results are given in Table IV. Moreover, these results may refer either to the site 1 or to the site 2, so that all together, we have four solutions compatible with the experimental data as for the orientations of **g** and **D** with regard to the bis heterobinuclear entity. We shall show in the next section that one of the solutions is physically much more likely than the other three.

Discussion

The magnetic behavior described in the previous section is intrinsic to the Cu(salen)Ni(hfa)$_2$ unit. The metal ions are antiferromagnetically coupled with a doublet–quartet separation of 35.4 cm^{-1}. This separation is much smaller than in CuNi(fsa)$_2$en(H$_2$O)$_2$·H$_2$O ($3J/2 \simeq -213$ cm^{-1}) owing to the weaker overlap of the x^2-y^2 type magnetic orbitals centered on copper and nickel, respectively, through the bent bridging network.[2,20,21] The absence of any sign of interaction between two symmetry-related CuNi pair is not surprising. Indeed, such an interaction would require an overlap of δ type between the x^2-y^2 orbitals centered on the copper atoms. Such an overlap for copper atoms separated by 3.432 Å is known to be extremely weak.

The $g_{1/2}$ and $g_{3/2}$ tensors associated with the low-lying pair states may be related to the local tensors $\mathbf{g}_{Cu}$ and g_{Ni} of the interacting ions through the spin Hamiltonian including the Zeeman perturbation for the CuNi unit noted A. This Hamiltonian is

$$\mathcal{H} = \mathcal{H}^A + \mathcal{H}_{ZE}$$

with

$$\mathcal{H}^A = \hat{S}^A_{Cu}\cdot\mathbf{J}^A_{CuNi}\cdot\hat{S}^A_{Ni} + \hat{S}^A_{Ni}\cdot\mathbf{D}^A_{Ni}\cdot\hat{S}^A_{Ni} \quad (3)$$

$$\mathcal{H}_{ZE} = \beta H(\mathbf{g}_{Cu}\cdot\hat{S}^A_{Cu} + \mathbf{g}_{Ni}\cdot\hat{S}^A_{Ni}) \quad (4)$$

$\mathbf{J}^A_{CuNi}$ is a dyadic taking into account isotropic, anisotropic, and antisymmetric interactions and $\mathbf{D}^A_{Ni}$ is the local zero-field-splitting tensor for the nickel(II) ion. The relationships between the $\mathbf{g}_{1/2}$ and $\mathbf{g}_{3/2}$ tensors and the local $\mathbf{g}_{Cu}$ and $\mathbf{g}_{Ni}$ tensors have been reported for the general case.[22,24] In the limit where the isotropic

(18) Wasserman, E.; Snyder, L. C.; Yager, W. A. *J. Chem. Phys.* **1964**, *41*, 1763–1772.
(19) Bencini, A.; Gatteschi, D. "Transition Metal Chemistry"; Nelson, G. A.; Figgis, B. M., Eds.; Marcel Dekker: New York, 1982; Vol. 8, pp 9–16.
(20) Charlot, M. F.; Jeannin, S.; Jeannin, Y.; Kahn, O.; Lucrêce-Abaul, J.; Martin-Frère, T. *J. Inorg. Chem.* **1979**, *18*, 1675–1681.
(21) Kahn, O.; Charlot, M. F. *Nouv. J. Chim.* **1980**, *4*, 567–576.
(22) Bencini, A.; Gatteschi, D. *Mol. Phys.* **1985**, *54*, 969–677.
(23) Hathaway, B. J.; Billing, D. E. *Coord. Chem. Rev.* **1970**, *5*, 143–207.
(24) Hulliger, J. Ph.D. Thesis, University of Zürich, Zürich, Switzerland, 1984.

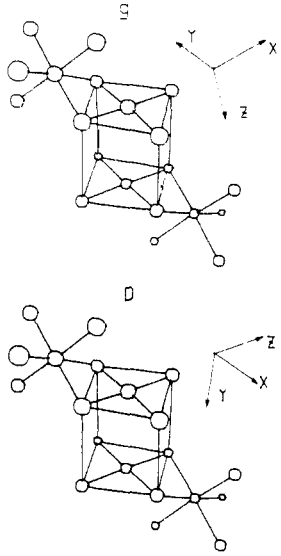

Figure 8. Orientations of **g** and **D** with regard to the bis heterobinuclear entity.

exchange within the CuNi pair $J = {}^1/_3 Tr J^{A}_{CuNi}$ is the leading term in (3), which is consistent with the magnetic properties, we have

$$\mathbf{g}_{1/2} = {}^1/_3(4\mathbf{g}_{Ni} - \mathbf{g}_{Cu})$$
$$\mathbf{g}_{3/2} = {}^1/_3(2\mathbf{g}_{Ni} + \mathbf{g}_{Cu}) \quad (5)$$

from $\tilde{g}_{1/2}$ and $\tilde{g}_{3/2}$, we can obtain the average local g values as

$$\bar{g}_{Cu} = 2.14$$
$$\bar{g}_{Ni} = 2.26$$

which compare well with the expected or reported values.[19,22-24] This result is not unexpected since it has been shown that **g** is not very sensitive to the D^{A}_{Ni}/J ratio, at least in the antiferromagnetic case,[22,24] so that eq 5 can be used for this purpose with some confidence.

In contrast with the magnetic susceptibility, the EPR "sees" the bis heterobinuclear entity noted here AB, A, and B representing each of the CuNi units. The first problem to solve is to choose between the four solutions for **g** and **D** compatible with the experimental data. **g** may be expressed as

$$\mathbf{g} = {}^1/_2(\mathbf{g}_A + \mathbf{g}_B) \quad (6)$$

where $\mathbf{g}_A$ and $\mathbf{g}_B$ refer to the doublet pair states for the Cu(salen)Ni(hfa)$_2$ unit. Since the two A and B units are related by a symmetry center, **g** will have the same principal directions as $\mathbf{g}_A$ and $\mathbf{g}_B$. From (5) we have

$$\mathbf{g}_A = {}^1/_3(4\mathbf{g}_{Ni} - \mathbf{g}_{Cu}) \quad (7)$$

The nickel(II) ion is in octahedral surroundings, so that $\mathbf{g}_{Ni}$ may be assumed to be almost isotropic.[19] So, the anisotropy of $\mathbf{g}_A$ will essentially reflect the anisotropy of $\mathbf{g}_{Cu}$. For a copper(II) ion in planar surroundings, g_{Cu_z} is the largest principal value of $\mathbf{g}_{Cu}$, z being the direction perpendicular to the CuN_2O_2 plane. The other two principal values, g_{Cu_x} and g_{Cu_y}, are oriented along the bonds in the CuN_2O_2 plane. It follows that, from (6), the orientation of **g** is expected to be as shown in **1**, with g_z smaller than g_x and g_y. Only one of the four possible solutions is close to the situation

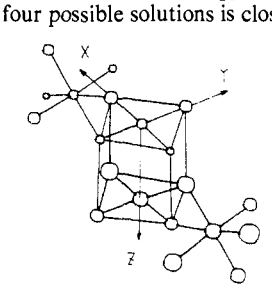

1

represented in **1**. It corresponds to the first fitting of Table IV and refers to the site of which the coordinates are given in Table II. g_z then makes an angle of 10.5° with the Cu1Cu'1 direction, g_x an angle of 5° with the Cu102 direction, and g_y an angle of 12.5° with the Cu101 direction. The orientations of **g** and **D** for this solution are represented in Figure 8. As expected since Wasserman's equations do not hold here, the two tensors are not coincident; g_u and D_u ($u = x, y$, and z) make an angle of about 20°.

Table V. Principal Values and Orientations with Regard to the *abc** Referential of the $\mathbf{D}^{dip}$ Tensor

0.0018	−0.4540	0.5895	0.6682
0.0007	−0.8166	0.0248	−0.5767
−0.0025	−0.3566	−0.8074	0.4700

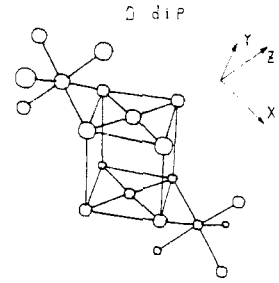

Figure 9. Orientation of $\mathbf{D}^{dip}$ with regard to the bis heterobinuclear entity (see text).

The problem at hand now is the origin of the zero-field splitting within the triplet state of the bis heterobinuclear entity. To approach this problem, it is convenient to consider an Hamiltonian

$$\mathcal{H} = \hat{S}_A \cdot \mathbf{J}_{AB} \cdot \hat{S}_B \quad (8)$$

expressing the interaction between the two ground doublet pair states and to relate the J_{AB} dyadic to those occurring in the complete exchange Hamiltonian

$$\mathcal{H} = \mathcal{H}^A + \mathcal{H}^B + \mathcal{H}^{AB} \quad (9)$$

with

$$\mathcal{H}^{AB} = \hat{S}^A_{Cu} \cdot \mathbf{J}^{AB}_{CuCu} \cdot \hat{S}^B_{Cu} + \hat{S}^A_{Ni} \cdot \mathbf{J}^{AB}_{NiNi} \cdot \hat{S}^B_{Ni} + \hat{S}^A_{Cu} \cdot \mathbf{J}^{AB}_{CuNi} \cdot \hat{S}^B_{Ni} + \hat{S}^A_{Ni} \cdot \mathbf{J}^{AB}_{NiCu} \cdot \hat{S}^B_{Cu} \quad (10)$$

where the meaning of the symbols is obvious. In the Appendix, there is established a general relationship between $\mathbf{J}_{AB}$ and the other $\mathbf{J}^{AB}_{ij}$ dyadics appearing in (10) and shown that in the limit where the isotropic exchange parameter J is dominant in $\mathcal{H}^A$ and $\mathcal{H}^B$, we have

$$\mathbf{J}_{AB} = \frac{1}{9}\mathbf{J}^{AB}_{CuCu} + \frac{16}{9}\mathbf{J}^{AB}_{NiNi} - \frac{4}{9}\mathbf{J}^{AB}_{CuNi} - \frac{4}{9}\mathbf{J}^{AB}_{NiCu} \quad (11)$$

This relation (11) holds for the isotropic parts of the **J**'s as well as for the anisotropic parts, which allows us to calculate the dipolar contribution to the zero-field splitting by using the approximation of the point magnetic dipoles. Such an approximation has been used for many copper(II) binuclear complexes.[25-29] For the calculation,[30-32] we used an isotropic g_{Ni} value of 2.26 and the g_{Cu_z}

(25) Felthouse, T. R.; Laskowski, E. J.; Hendrickson, D. N. *Inorg. Chem.* **1977**, *16*, 1077-1089.
(26) Damoder, R.; More, K. M.; Eaton, G. R.; Eaton, S. S. *J. Am. Chem. Soc.* **1983**, *105*, 2147-2154.
(27) Banci, L.; Bencini, A.; Gatteschi, D. *J. Am. Chem. Soc.* **1983**, *105*, 761-764.
(28) Bencini, A.; Gatteschi, D.; Zanchini, C. *Inorg. Chem.*, in press.
(29) Boillot, M. L.; Journaux, Y.; Bencini, A.; Gatteschi, D.; Kahn, O. *Inorg. Chem.* **1985**, *24*, 263-267.
(30) Owen, J.; Harris, E. A. "Electron Paramagnetic Resonance"; Geshwind, S., Ed.; Plenum Press: New York, 1972; pp 427-492.
(31) Abragam, A.; Bleaney, B. "Electron Paramagnetic Resonance of Transition Ions"; Clarendon Press: New York, 1970; pp 492-495.
(32) Boyd, P. D.; Toy, D.; Smith, T. D.; Pilbrow, J. R. *J. Chem. Soc., Dalton Trans.* **1973**, 1549-1563.

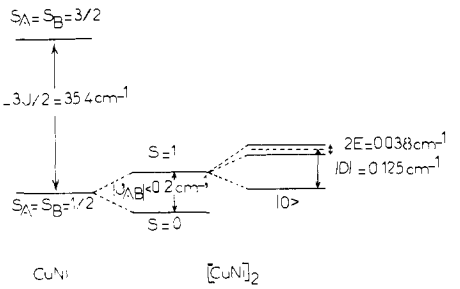

Figure 10. Low-lying states in $[Cu(salen)Ni(hfa)_2]_2$ (see text). It should be noticed that the experimental data cannot distinguish between $S = 0$ ($J_{AB} < 0$) as shown in the figure and $S = 1$ ($J_{AB} > 0$) for the ground state of the bis heterobinuclear entity.

$= 2.24$ and $g_{Cu_x} = g_{Cu_y} = 2.025$ values deduced from the powder EPR spectrum of Cu(salen). The principal values and the orientation of this $\mathbf{D}^{dip}$ tensor are given in Table V and visualized in Figure 9.

Comparing $\mathbf{D}^{dip}$ to the experimental $\mathbf{D}$ tensor shows that the former is much smaller than the latter and also that the principal directions are fairly different from each other. This difference may have two origins: (i) The ground state of a CuNi pair is not a rigorously pure doublet state. It contains a weak contribution from the quartet state located at 35.4 cm^{-1} above owing to the coupling of the components of the $S = {}^1/_2$ and ${}^3/_2$ states through the local anisotropy of the nickel(II) ion. In other words, the ground state of the CuNi pair cannot be treated exactly as the doublet ground state of a copper(II) compound. In the Appendix, it is shown that this $S = {}^1/_2$, ${}^3/_2$ mixing contributes to the zero-field splitting within the triplet state of the $|CuNi|_2$ entity. This contribution varies as D^A_{Ni}/J on the one hand and as J_{AB} on the other hand. To specify the magnitude of this effect, we performed a calculation with several values of the axial anisotropy parameter D^A_{Ni} ranging from 1 to 5 cm^{-1}, the actual J value and $|J_{AB}| = 0.2$ cm^{-1}, which will be shown to be the upper limit for J_{AB}, and we found D_z varying from 0.017 to 0.081 cm^{-1}, which is of the same order of magnitude as the observed value (0.078 cm^{-1}) and anyhow far from being negligible. (ii) The anisotropic exchange is due to the combined effect of the spin–orbit coupling within a CuNi pair and the interaction between the ground state of a CuNi pair and the excited states of the other pair.[2,10,19,35] This anisotropic exchange has recently been shown to be the main contribution to the zero-field splitting within the triplet state of copper binuclear complexes, with magnitudes also of the same order as what is found in our compound.[27,29] To summarize, it appears difficult to specify the relative contributions of these two effects which however are likely both operative.

Conclusion

If the molecular structure of $Cu(salen)Ni(hfa)_2$ itself is not exceptional, the repetition of the molecular unit gives rise to quite a remarkable bis heterobinuclear entity $|CuNi|_2$ with a rather short Cu–Cu separation. This peculiar packing raises a question; namely, has this bis heterobinuclear structure any consequence on the physical properties of the compound in the solid state? This paper is devoted to this problem. We investigated both the magnetic and the EPR properties. As far as the magnetic behavior is concerned, the compound behaves exactly as it is expected for a $Cu(salen)Ni(hfa)_2$ complex with a doublet ground state and a quartet excited state located at 35.4 cm^{-1} above. In other words, the packing of two symmetry-related CuNi units has no consequence on the magnetic properties down to 1.27 K. The interaction between two doublet pair states within the bis heterobinuclear entity should give rise to both a singlet–triplet (S–T) splitting and a zero-field splitting of the triplet state. The magnitude of this latter effect is known from the EPR study. The axial and rhombic zero-field-splitting parameters are $|D| = 0.125$ cm^{-1} and $|E| = 0.019$ cm^{-1}, respectively. It is then possible to obtain an upper limit for the S–T splitting, using the theoretical expression of the magnetic susceptibility for two interacting doublet states and assuming that the resulting singlet is the lowest, as it is likely. This limit is 0.2 cm^{-1}. It would be most interesting to extend the magnetic investigation much below 1.27 K, in order to obtain the actual value of the S–T splitting.

In contrast with the magnetic properties, the EPR properties are entirely associated with the bis heterobinuclear nature of the compound. Indeed, the EPR spectrum is that of a low-lying triplet state, with zero-field splitting and forbidden half-field transition. *This state arises from the interaction between two doublet pair states.* To our knowledge, such a situation has never been reported before. It is likely worthwhile to point out that the triplet state detected in EPR cannot be described as arising from a copper(II)–copper(II) interaction within the 0102N6N50′10′2N′6N′5 square prism. If it was so, $\mathbf{g}_A$ and $\mathbf{g}_B$ in (6) would be the local tensors for the copper(II) ions in planar surroundings and $\mathbf{g}$ would be oriented with its largest principal value along the Cu1Cu′1 direction. None of the four solutions compatible with the experimental data corresponds to that. In a sense, $[Cu(salen)Ni(hfa)_2]_2$ shows the same contrast between magnetic and EPR properties as $[Cu(pyO)(NO_3)_2]_2$. The magnetic susceptibility data on this compound down to 1.2 K failed to show the presence of any interaction between the two metal ions[33] whereas the EPR spectra were unambiguously those of a triplet state.[34]

We attempted to specify the mechanism of the zero-field splitting within the triplet state of the bis heterobinuclear unit. For that, we presented a model allowing the calculation of the dipolar contribution $\mathbf{D}^{dip}$, which was found to be only a very weak component of the observed $\mathbf{D}$ tensor. This difference is ascribed to both the specific nature of the interacting doublet states in which the local anisotropy of the nickel(II) ion may play a significant role and the anisotropic exchange. We have developed a model that takes into account the specificity of the interacting doublet states to describe this interaction. From this model, it is apparent that along with the anisotropic exchange, the combined effect of the local anisotropy of the nickel(II) ions and the isotropic exchange between the CuNi pairs has an effect on the zero-field splitting within the triplet state of the $|CuNi|_2$ entity.

To conclude, we would like to emphasize quite the heuristic complementarity of the magnetic and EPR techniques to study the electronic structure of the heteropolymetallic systems. In the present case, this complementarity allows us to represent the low-lying levels in $[Cu(salen)Ni(hfa)_2]_2$ as shown in Figure 10, where the interaction between the symmetry-related $Cu(salen)Ni(hfa)_2$ units appears as a weak perturbation with regard to the dominant interaction between copper(II) and nickel(II) ions within the CuNi unit.

Acknowledgment. This work is supported by the NATO research Grant 0271/83. We are most grateful to J. J. Girerd for very stimulating discussions and to J. P. Renard who measured the magnetic data in the 1.27–4.2 K temperature range.

Appendix

In order to relate the $\mathbf{J}_{AB}$ dyadic appearing in (8) to those of (10), we use a previously reported procedure[22,24] according to which the ground Kramers doublet for a CuNi pair can be represented by an operator $\hat{S}_k$. This operator is related to the single-ion spin operators by

$$\hat{S}^K_i = \mathbf{M}^K_i \hat{S}_K \quad (i = Cu, Ni;\ K = A, B) \tag{12}$$

The $\mathbf{M}^K_i$ matrices have been reported for the general case and for some special cases.[22,24] Substituting (12) into (10) and considering $\mathbf{J}^{AB}_{CuNi} = \mathbf{J}^{AB}_{NiCu}$, we obtain

$$\hat{J}_{AB} = 2(\tilde{\mathbf{M}}^A_{Cu}\cdot\mathbf{J}^{AB}_{CuNi}\cdot\mathbf{M}^B_{Ni}) + \tilde{\mathbf{M}}^A_{Cu}\cdot\mathbf{J}^{AB}_{CuCu}\cdot\mathbf{M}^B_{Cu} + \tilde{\mathbf{M}}^A_{Ni}\cdot\mathbf{J}^{AB}_{NiNi}\cdot\mathbf{M}^B_{Ni} \tag{13}$$

In the limit where $|J|$ is much larger than D^A_{Ni} ($= {}^3/_2 D^A_{Ni_z}$) and where the interaction is antiferromagnetic, we have

(33) Carlin, R. L.; Burriel, R.; Corneliesse, R. M.; Van Duyneveldt, A. J. *Inorg. Chem.* **1983**, *22*, 831–832.
(34) Hatfield, W. E. *Inorg. Chem.* **1983**, *22*, 833–837.
(35) Moriya, T. *Phys. Rev.* **1960**, *120*, 91–98.

$$M^K_{Cu_u} = -1/3$$

$$M^K_{Ni_u} = 4/3 \quad u = x, y, z \quad K = A, B$$

and (13) becomes (11). In the general case, the M_i^K matrices are not isotropic but have quite a general form. The components of J_{AB} can then be expressed according to

$$J_{AB_{uv}} = \sum_{KK'} \sum_{lm} \tilde{M}^A_{Kul} (J^{AB}_{KK'}\delta_{lm} + D^{AB}_{KK'lm}) M^B_{K'mv} \quad (14)$$

where $K, K' \equiv$ Cu, Ni, l and m run from 1 to 3, $J^{AB}_{KK'} = {}^1/_3 Tr(\mathbf{J}^{AB}_{KK'})$ and $\mathbf{D}^{AB}_{KK'} = \mathbf{J}^{AB}_{KK'} - J^{AB}_{KK'}\mathbf{I}$ where I is the identity matrix. From (14), it clearly appears that when the $\mathbf{M}_i^K$ matrices are not isotropic, the isotropic parts of the $\mathbf{J}^{AB}_{KK'}$ dyadics can contribute to the anisotropic components of $\mathbf{J}_{AB}$.

Registry No. Cu(salen)Ni(hfa)$_2$, 71073-29-5; Cu(salen), 14167-15-8; Ni(hfa)$_2$(H$_2$O)$_2$, 98088-59-6.

Supplementary Material Available: Listing of structure factor amplitudes, the thermal parameters for non-hydrogen atoms (Table VI), and the positional and thermal parameters for hydrogen atoms (Table VII) (32 pages). Ordering information is given on any current masthead page.

Combinational *O*-Aryl Carbamate and Benzamide Directed Ortho Metalation Reactions. Synthesis of Ochratoxin A and Ochratoxin B

Mukund P. Sibi, S. Chattopadhyay, John W. Dankwardt, and V. Snieckus*

Contribution from the Guelph-Waterloo Centre for Graduate Work in Chemistry, University of Waterloo, Waterloo, Canada N2L 3G1. *Received April 5, 1985*

Abstract: The syntheses of isocoumarins **9a** and **9b**, known penultimate precursors for the toxic fungal metabolites ochratoxin B (**3a**) and ochratoxin A (**3b**), respectively, are reported. The syntheses are initiated from *O*-aryl carbamates **4a,b** and proceed through intermediates **5c,d**, **7c,d**, and **8b,c** by a synthetic design that involves comprehensive application of the directed ortho metalation reaction on *O*-aryl carbamates and tertiary benzamides.

Directed metalation-derived ortho-lithiated benzamides,[1] and more recently, the corresponding *O*-aryl carbamates,[2] are becoming recognized as useful synthons for the regioselective construction of diverse polysubstituted aromatics.[3] Herein we report the combinational use of carbamate- and amide-directed ortho metalation reactions to achieve rapid access to multifunctional aromatic systems according to Scheme I.

In this synthetic design, involving comprehensive use of aromatic metalation, the first electrophile (E_1^+) introduced into the ortho-lithiated carbamate **1** (step 1) is chosen to be compatible with subsequent metalation conditions and/or a weaker ortho director than the carbamate.[4] This forces the second metalation into the alternative ortho site, thereby triggering 1,3-carbamoyl rearrangement (step 2).[2] Following phenol protection (PG), the third metalation is directed by the migrated amide, leading to regiospecific E_2^+ introduction (step 3) (especially if R = OMe),[1] thus concluding the construction of a contiguously tetra- or pentasubstituted system (**2**). The utility of this conceptualization is demonstrated in short syntheses of ochratoxin A (**3b**)[5] and ochratoxin B (**3a**),[5] toxic metabolites isolated from strains of *Aspergillus ochraceus* and *Penicillium viridicatum*, which constitute human and animal health hazards owing to their presence in agricultural products.[6-9]

Scheme I

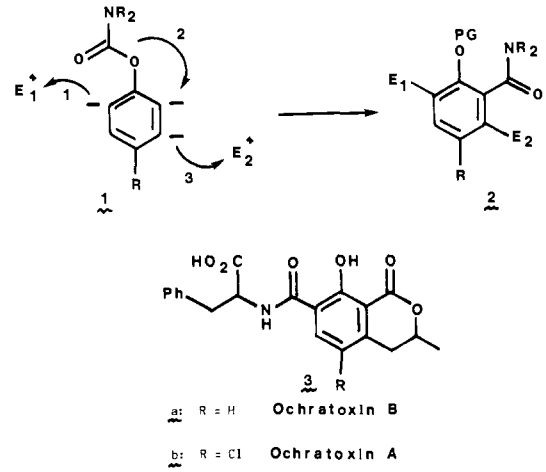

Metalation of the readily accessible *O*-aryl carbamate **4a** with *sec*-BuLi/TMEDA under the widely recognized standard conditions (THF/-78 °C) followed by quenching with carbon dioxide[2] provided the benzoic acid **5a** in excellent yield (Scheme II). Under identical conditions, the chloro carbamate **4b** smoothly afforded compound **5b** in somewhat lower yield. Carbamate O-to-C 1,3-migration in **5a** was effected also under the standard *sec*-BuLi/TMEDA (2 equiv) metalation conditions followed by slow warming to room temperature[2] to give the intermediate phenol **6a**.[10] For convenience in purification, **6a** was methylated, a step that required a subsequent base-catalyzed hydrolysis to reverse the unavoidable formation of the methyl ester. The final product **7a** was thereby obtained in modest yield.[11]

(1) Beak, P.; Snieckus, V. *Acct. Chem. Res.* **1982**, *15*, 306.
(2) Sibi, M. P.; Snieckus, V. *J. Org. Chem.* **1983**, *48*, 1935.
(3) For recent methodological and target-oriented endeavors, see: Snieckus, V. *Lect. Heterocycl. Chem.* **1984**, *7*, 95.
(4) Intramolecular competition metalation experiments between carbamate and amide have shown that the former is a somewhat better ortho director: Miah, M. A. J.; Snieckus, V., unpublished results.
(5) Previous syntheses: (a) Steyn, P. S.; Holzapfel, C. W. *Tetrahedron* **1967**, *23*, 4449; (b) Roberts, J. C.; Woollven, P. *J. Chem. Soc. C* **1970**, 278; (c) Kraus, G. A. *J. Org. Chem.* **1981**, *46*, 201.
(6) For other, simply modified ochratoxin metabolites, see: Nakanishi, K.; Goto, T.; Ito, S.; Natori, S.; Nozoe, S. "Natural Product Chemistry"; Kodansha Ltd. (Tokyo) and Academic Press (New York), 1975; Vol. II, p 198.
(7) Korgh, P. In "Mycotoxins in Human and Animal Health"; Rodricks, J. V., Hesseltine, C. W., Mehlman, M. A., Eds.; Pathotox Publishers: Fark Forest South, IL, 1977; p 489.
(8) Wood, G. M. *Chem. Ind (London)* **1982**, 972.
(9) For biosynthesis, see: Vleggaar, R.; Steyn, P. S. In "The Biosynthesis of Mycotoxins"; Steyn, P. S., Ed.; Academic Press: New York, 1980; p 395.
(10) That the potentially expected ketone formation from the reaction of a benzoic acid with *sec*-BuLi does not constitute a problem has been previously demonstrated; see: Beak, P.; Brown, R. A. *J. Org. Chem.* **1982**, *47*, 34.
(11) Attempts at a further abbreviation by forming the *O,O,C* trianion of **6a**, R = H, in situ failed. See also: Billedeau, R. J.; Sibi, M. P.; Snieckus, V. *Tetrahedron Lett.* **1983**, 4515.

0002-7863/85/1507-6312$01.50/0